Spin- and valley-polarized transport and magnetoresistance in asymmetric ferromagnetic WSe_2 tunnel junctions

Yaser Hajati[*] and Mohammad Alipourzadeh[†]
Department of Physics, Faculty of Science, Shahid Chamran University of Ahvaz, Ahvaz 6135743135, Iran

Imam Makhfudz[‡]
GREMAN, UMR 7347, Universite de Tours, Parc de Grandmont, Tours 37200, France

(Received 5 April 2021; revised 8 June 2021; accepted 15 June 2021; published 28 June 2021)

Transition metal dichalcogenides (TMDs) offer a new platform for theoretical study of two-dimensional materials and their applications, beyond graphene. Previous studies indicate that monolayers of TMDs become ferromagnetic when put in proximity to conventional ferromagnetic, leading to remarkable spin and valley transport properties when combined with the intrinsic spin-orbit coupling (SOC) inherent in these materials. In this work, we show that a magnetic tunnel junction setup consisting of an asymmetric ferromagnetic/ferromagnetic/normal WSe_2 junction gives rise to a fully spin- and valley-polarized current for both parallel and antiparallel magnetization configurations in the presence of an off-resonance light. Due to the strong SOC of WSe_2 together with off-resonance light, both the spin and valley polarizations are tunable and switchable. We also find that the tunneling magnetoresistance (TMR) could be tuned to 1 by off-resonance light. The relatively much stronger SOC in the conduction and valence bands of WSe_2 compared to other compounds of the dichalcogenides family in collaboration with an off-resonance light leads to significant negative TMR at weak enough exchange fields. In appropriate parameter regimes, the TMR oscillations from negative to positive values can be tuned by the off-resonance light. Our results suggest that magnetic tunnel junctions involving WSe_2 have very promising potential for applications in magnetic memory and spin and valleytronics devices.

DOI: 10.1103/PhysRevB.103.245435

I. INTRODUCTION

Monolayer transition metal dichalcogenides (TMDs) (e.g., MX_2, where M = Mo, W; X = S, Se, and Te) are attractive materials for spintronics and valleytronics applications, due to their strong spin-orbit interaction [1–3] and huge direct band gap [4]. In TMDs, the conduction and valence band extrema are located at two degenerate valleys (K, K') at the corners of the first hexagonal Brillouin zone [5]. The broken inversion symmetry and strong spin-orbit coupling (SOC) in TMDs lead to coupling of spin and valley degrees of freedom, where the spin splitting of the valence band is opposite at the two valleys, as required by time-reversal symmetry [6–9]. One of the most important issues in realization of two-dimensional materials is the generation of fully spin and valley polarizations. Among many TMDs, a high quality of WSe_2 with strong SOC of 450 meV in the valence band's edge and 30 meV in the conduction band's edge is an excellent material for achieving fully spin and valley polarizations. In addition, a monolayer WSe_2 is a direct band-gap semiconductor of ($2\Delta = 1.7$ eV) [10] which makes it a very suitable platform for developing novel spintronics and valleytronics devices through manipulating the spin and valley degrees of freedom.

Recently, Zhao *et al.* have shown that in WSe_2/EuS, the magnetic proximity effect results in a giant valley splitting for monolayer WSe_2, which is enhanced by nearly two orders of magnitude higher than that obtained by an external magnetic field [11]. Seyler *et al.* also showed valley splitting and polarization in WSe_2/CrI_3 [12]. Both of these results suggest the possibility of controlling the valley degrees of freedom in a feasibly low-magnetic field using magnetic proximity effect. Qiu *et al.* have shown that due to the band gaps of valley K and K' responding differently to off-resonant light together with the huge SOC in WSe_2, the perfect valley and spin polarizations are obtained [13]. Tahir *et al.* have shown that in normal/ferromagnetic/normal (NFN) based WSe_2 junctions, the Zeeman field opens different spin-dependent band gaps at the K and K' valleys, which in turn induce spin- and valley-polarized transport [5].

Tunneling magnetoresistance (TMR) is another important quantity in spintronics which has many applications in magnetic random access memory (MRAM) [14], hard disk drive (HDD) [15], and magnetic sensors [16]. Transport properties of WSe_2 with strong SOC display novel behaviors different from those in other TMDs and two-dimensional materials. So far, spin and valley polarizations and TMR have been studied extensively in many ferromagnetic junctions based on graphene [17,18], silicene [19–22], and MoS_2 [23–27]. However, transport properties of an asymmetric ferromagnetic/ferromagnetic/normal (FFN) WSe_2 junction have not yet been considered in the literature. In

[*]yaserhajati@scu.ac.ir
[†]m.alipourzadeh@gmail.com
[‡]imakhfudz@gmail.com

this paper, we study charge conductance and spin and valley polarizations along with TMR in an asymmetric FFN WSe_2 junction. Here, we demonstrate full spin and valley polarizations for both parallel and antiparallel configurations along with TMR through FFN WSe_2 junction in the presence of gate voltage and off-resonance circularly polarized light. It is found that circularly polarized light lifts both the spin and valley degeneracies which are due to the SOC in the edges of valence and conduction bands of WSe_2. As a result, at some values of gate voltage, the spin polarizations can be switched by changing the polarity of off-resonance light, which has not been reported in the similar ferromagnetic-TMDs junctions [23]. The relatively much stronger SOC in the conduction and valence bands of WSe_2 compared to other compounds of the dichalcogenide family in collaboration with an off-resonance light leads to significant negative TMR at weak enough exchange fields, a finding which has not been reported in other asymmetric FFN junctions based on silicene [20] and MoS_2 [23]. We find that in some parameter regimes, the TMR oscillates from negative to positive values with respect to the length of the middle ferromagnetic region (L) and amplitude of these oscillations can be controlled by the off-resonance light.

II. HAMILTONIAN AND SCATTERING MATRIX THEORY OF WSe_2 JUNCTION

The proposed asymmetrical FFN WSe_2 junction has shown schematically in Fig. 1(a), where electrostatic gate potential and off-resonant circularly polarized light are placed in the central ferromagnetic region. Here, ferromagnetism in WSe_2 is induced through proximity effect when it is placed in proximity with a ferromagnetic layer, similar to what reported in graphene [28], silicene [19,20], MoS_2 [23,25], and topological insulators [29]. Recent experimental [6,30–32] and theoretical [10,13,33] studies have shown the effect of circularly polarized light on valley polarization in monolayer TMDs. The circularly polarized light is described by an electromagnetic potential as $\boldsymbol{A}(t) = [A\sin(\pm\Omega t), A\cos(\pm\Omega t)]$, where Ω is the frequency of light and the plus (minus) sign corresponds to the right-handed (left-handed) circular polarization and $A = E_0/\Omega$ with E_0 being the amplitude of the electric field. In this regime, the light does not directly excite the electrons and instead effectively modifies the electron band structure through virtual photon absorption and emission processes [34,35]. Based on the Floquet theory [36], the effect of time-related electromagnetic potential from the light is reduced to a static effective Hamiltonian. For $eAv_f/\Omega \ll 1$ (where $v_f = 5\times10^5$ m/s is the Fermi velocity in WSe_2), the low-energy Hamiltonian for the proposed WSe_2 junction is given by [7,13]

$$H = \hbar v_f(\eta k_x\sigma_x + k_y\sigma_y) + [\Delta + \eta\Delta_\Omega(x) + \eta s_z\lambda_-]\sigma_z + (\eta s_z\lambda_+) + U(x) - s_z h(x), \quad (1)$$

where $\Delta_\Omega = (ev_fA)^2/\hbar\Omega$ is the effective energy term describing the effects of the circularly polarized light, which essentially renormalizes the mass of the Dirac fermions. Here, $s_z = \pm1$ denotes the electron spin up and spin down, $\eta = \pm1$ corresponds to the K and K' valley points, and $\sigma_{x,y,z}$ represents the Pauli matrix in the sublattice space. We define $\lambda_\pm = (\lambda_c \pm \lambda_v)$ where $4\lambda_c = 30$ meV and $4\lambda_v = 450$ meV are the spin splitting at the edges of conduction and valence bands, respectively, caused by the intrinsic SOC. According to the Floquet theory, the light must satisfy the condition $\hbar|\Omega| \gg t$, where $t = 1.1$ eV is the hopping parameter between two nearest neighbors of WSe_2. The lowest frequency is determined by the bandwidth $3t \approx 800$ THz for WSe_2 [34]. The typical experimental field strength can be considered as $eA = 0.01$ Å^{-1}, as reported previously in semi-Dirac material [37], and corresponds to the laser intensity $I = (eA\Omega)^2/8\pi\alpha\hbar \sim 3\times10^8$ W/(cm^2), where α is the fine-structure constant. Although this intensity is still considered as a high intensity, we can assume this light source as pulse irradiation, which can be less destructive, due to not irradiating continuously.

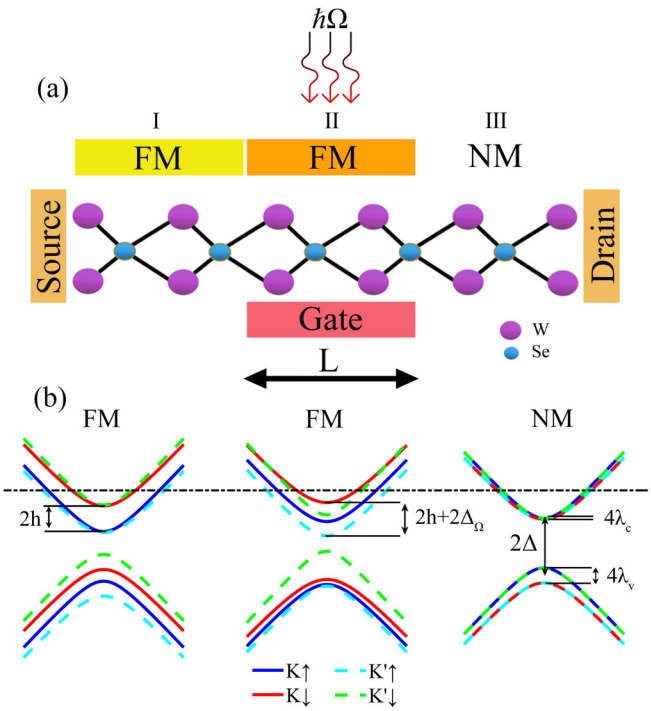

FIG. 1. (a) Schematic diagram of WSe_2-based FFN junction and (b) band structure near Dirac points (K, K') for both spin and valleys. The horizontal black line denotes the Fermi level E_F.

The electrostatic gate potential and off-resonance light in the middle region can be defined through the Heaviside step function $[\Theta(x)]$ as $U(x) = U\Theta(x)\Theta(x-L)$ and $\Delta_\Omega(x) = \Delta_\Omega\Theta(x)\Theta(L-x)$, respectively. Also, the exchange splitting in the two ferromagnetic regions can be described as $h(x) = h_1\Theta(-x) \pm h_2\Theta(x)\Theta(L-x)$, where h_1 (h_2) is the exchange splitting induced by the left (middle) ferromagnetic region and $\pm$ corresponds to the parallel (P) and the antiparallel (AP) configurations of magnetization. $\Delta = 850$ meV is the mass term that breaks the inversion symmetry. The eigenvalue of the Hamiltonian in the middle ferromagnetic region is given by

$$E = \pm\sqrt{(\hbar v_f k')^2 + (\Delta_{\eta,s_z})^2} + U_{\eta,s_z}, \quad (2)$$

where $\Delta_{\eta,s_z} = \Delta + \eta\Delta_\Omega(x) + \eta s_z\lambda_-$, $U_{\eta,s_z} = s_z[\eta\lambda_+ - h(x)] + U(x)$, and $\pm$ represents the conduction and valence

band, respectively. In the normal region, the eigenvalue can be acquired by setting $U = h = \Delta_\Omega = 0$ and also in the left ferromagnetic region by setting $U = \Delta_\Omega = 0$. Here, we assume k, k', and k'' as the wave vector in left, center, and right layer, respectively. The general form of wave function is

$$\psi_{(x)} = \alpha_{\eta,s_z}\begin{pmatrix}\hbar v_f k'_- \\ E_v\end{pmatrix} e^{ik'_x x} e^{ik'_y y} + \beta_{\eta,s_z}\begin{pmatrix}-\hbar v_f k'_+ \\ E_v\end{pmatrix} e^{-ik'_x x} e^{ik'_y y}, \tag{3}$$

with $k'_\pm = \eta k'_x \pm i k'_y$, $E_v = E - \Delta - (\eta s_z \lambda_-) - (\eta s_z \lambda_+) + s_z h_2 - U - \eta\Delta_\Omega$, and k'_x and k'_y are the perpendicular and parallel wave-vector components of electron in the middle ferromagnetic region. Because of the translational invariance, all transverse wave vectors during the scattering process are conserved. The transmission probability can be calculated using the condition of continuity of wave functions at the boundaries ($x = 0, L$).

The normalized spin- and valley-resolved conductances at zero temperature are evaluated according to the standard Landauer-Buttiker formalism as [38,39]

$$G_{\eta,s_z} = G_0 \frac{\hbar v_f k}{E_F} \int_{-\phi_c}^{\phi_c} T_{\eta,s_z} \cos\phi \, d\phi, \tag{4}$$

where $G_0 = e^2 L_y E_F/(2\pi\hbar h v_f)$ is the reduced unit of conductance with the system transverse length L_y and ϕ_c is the critical incident angle of electrons. Propagating modes for k_x requires satisfying $\phi_c = \pi/2$ for $k \leqslant k''$ and $\phi_c = \arcsin(k''/k)$ for $k > k''$. The spin- and valley-resolved conductances are defined as $G_{\uparrow(\downarrow)} = (G_{K_{\uparrow(\downarrow)}} + G_{K'_{\uparrow(\downarrow)}})/2$ and $G_{K(K')} = (G_{K(K')_\uparrow} + G_{K(K')_\downarrow})/2$ and total charge conductance (G) is defined as $G = G_K + G_{K'} = G_\uparrow + G_\downarrow$. So, the valley ($P_v$) and spin ($P_s$) polarizations can be written as [40,41]

$$P_{v(s)} = \frac{G_{K(\uparrow)} - G_{K'(\downarrow)}}{G}, \tag{5}$$

Throughout this paper, we assumed that the magnetization orientation in the left ferromagnetic region is always in positive form, while that in the middle region can be reversed. This can lead to two types of magnetization configurations: parallel (P) and antiparallel (AP). Finally, the TMR can be calculated as

$$\mathrm{TMR} = \frac{G_\mathrm{P} - G_\mathrm{AP}}{G_\mathrm{P}}. \tag{6}$$

Note that the common form of Eq. (6) is like $\mathrm{TMR} = (G_\mathrm{P} - G_\mathrm{AP})/G_\mathrm{AP}$, but it also can be written as we wrote, which is used in Refs. [19,25,42] and we choose this form because in our work, G_AP vanishes at $\Delta_\Omega = E + h + \Delta + \lambda_- - \lambda_+$, which leads to an infinity in the TMR.

III. NUMERICAL RESULTS AND DISCUSSION

A. Spin and valley polarizations

Here, we apply the above formulation to calculate the spin and valley transports and TMR in an asymmetrical FFN WSe_2 junction in the presence of off-resonant circularly polarized light and gate voltage. Throughout the paper, we fix the Fermi energy $E = 1.7$ eV and the exchange field in the left ferromagnetic region $h_1 = 0.6$ eV. Note also that we set the gate voltage to zero except in Fig. 5. Before proceeding with the calculations, we discuss the band structure diagrams in Fig. 1(b). From Eq. (2), it can be seen that exchange field together with SOC, break spin and valley degeneracies, and the spin (valley) splitting has the same direction at both valleys (spin bands). In the normal WSe_2, the Fermi level crosses both spin (valley) bands, consequently, both spins (valleys) contribute to the conductance, leading to a nonpolarized transport.

Notably, the monolayer WSe_2 is feasible to fabricate by the mechanical exfoliation method of bulk WSe_2 [43,44]. In reality, disorder, impurities, and intervalley scattering by atomic defects in monolayer TMDs are common limiting factors for applications exploiting their unique valley properties. The static disorder like that induced by curvature or topological defect breaks the time-reversal symmetry around K and K' valleys and could be added to the effective Hamiltonian for each valley as a complex-conjugate operator times (σ_y), similar to those reported in Refs. [45,46]. Also, from a familiar experimental study on monolayer WSe_2, it is found that the disorder potential attributed to local strain and shallow impurity potentials reduces valley coherence but has less effect on valley polarization [47].

Note also that the alignment of the layers (in the FFN junction), ideally assumed to be aligned perfectly, is not always possible experimentally and this may lead to interfacial effects such as Rashba spin-orbit coupling in magnetic proximity effect in TMDs [48]. In general, our results are guaranteed to hold for clean enough samples, and Rashba SOC can be neglected [48]. Our results remain qualitatively robust against slight imperfections, impurities, misalignments, disorders, with the available experimental techniques where these nonidealities can be minimized.

To understand the role of the exchange field (off-resonance light) in the left (middle) ferromagnetic region, the low-energy dispersion relations at $k = 0$ are plotted in Fig. 2. It can be seen that in the presence of h_1, the spin and valley degeneracy breaking is more pronounced in the valence band (dotted curves) as compared with the conduction band (dashed and solid curves), because of the stronger SOC in the edge of the valence band ($\lambda_v = 112.5$ meV) as compared with conduction band ($\lambda_c = 7.5$ meV) [see Figs. 2(a) and 1(b)]. This finding is interesting because in the FFN MoS_2 junction we can not see similar behavior for electrons in the conduction band which is due to the lack of SOC in the conduction band of MoS_2 [23]. From the inset of Fig. 2(a), it is obvious that in the absence of h_1 ($h_1 = 0$) the spin splitting is opposite at different valleys, due to the SOC, which means $E_{K_\uparrow} = E_{K'_\downarrow}$ and $E_{K_\downarrow} = E_{K'_\uparrow}$ in both valence and conduction bands, manifestation of Kramers degeneracy. However, applying the exchange field ($h \neq 0$) gives rise to spin splitting in both valence and conduction bands, due to the time-reversal symmetry breaking induced by the exchange field, acting like a Zeeman field. This interaction between h and spin bands is expected from the spin index (s_z) beside the exchange field in Eq. (1).

Figures 2(b) and 2(c) show the conduction band energy of the middle ferromagnetic region versus Δ_Ω for the P and AP configurations, respectively. Importantly, the inversion symmetry breaking in WSe_2 selectively couples K' (K) for a

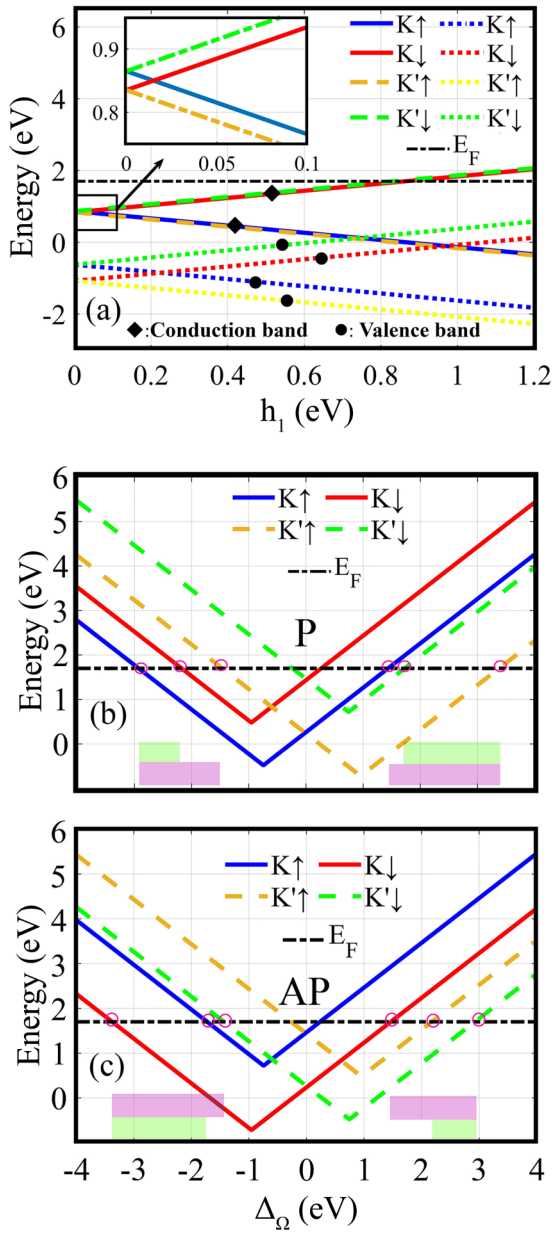

FIG. 2. (a) Conduction and valence energy bands near the K and K' valleys at $k = 0$ as a function of h_1, and (b), (c) conduction bands at $k = 0$ versus Δ_Ω. $h_2 = 0.6$ eV for (a)–(c) and $h_1 = 0.6$ eV for (a) and (b). The green (purple) rectangles denote spin-valley (valley) polarization window.

right- (left-) handed circularly polarized light as can be understood from Figs. 2(b) and 2(c). So, when $\Delta_\Omega = 0$, we can see $E_{K\downarrow} \approx E_{K'\downarrow}$ and $E_{K\uparrow} \approx E_{K'\uparrow}$ in the conduction band. It is noteworthy that, if we remove the SOC from the conduction band, then we have $E_{K\downarrow} = E_{K'\downarrow}$ and $E_{K\uparrow} = E_{K'\uparrow}$ for $\Delta_\Omega = 0$, similar to those reported in FFN MoS_2 [23]. Of course, the remaining spin splitting at $\Delta_\Omega = 0$ is due to the exchange field together with SOC in the central ferromagnetic region.

For a perfect spin (valley) polarization, the Fermi level should intersect with only one spin (valley) band. Due to the exchange field (off-resonance light) and existing intrinsic SOC, all bands will be separated, so Fermi level crosses one spin band from one valley, causing fully spin- and valley-polarized transport ($P_s = P_v = \pm 1$) for both P and AP configurations [green windows in Figs. 2(b) and 2(c)].

The condition to realize fully spin- and valley-polarized transport (spin-valley filter) can be obtained as follows: for the P conguration when $\Delta_\Omega \in [-(E_F + h + \Delta + \lambda_- - \lambda_+), -(E_F + \lambda_+ - h + \Delta - \lambda_-)]$, i.e., $\Delta_\Omega \in [-2.925, -2.175]$ and when $\Delta_\Omega \in [E_F - \lambda_+ - h + \Delta + \lambda_-, E_F + h + \Delta - \lambda_- + \lambda_+]$, i.e., $\Delta_\Omega \in [1.725, 3.375]$ only one spin-valley band crosses the Fermi level, causing the transmission to be dominated only by $K_\uparrow$ and $K'_\uparrow$ electrons, respectively [see the green windows in Fig. 2(b)]. Also, for the AP configuration when $\Delta_\Omega \in [-(E_F + h + \Delta - \lambda_- + \lambda_+, -(E_F - \lambda_+ - h + \Delta + \lambda_-)]$, i.e., $\Delta_\Omega \in [-3.375, -1.725]$ and when $\Delta_\Omega \in [E_F - h + \Delta - \lambda_- + \lambda_+, (E_F - \lambda_+ + h + \Delta + \lambda_-)]$, i.e., $\Delta_\Omega \in [2.175, 2.925]$ the transmission is handled only by $K_\downarrow$ and $K'_\downarrow$, respectively, due to the crossing of one spin-valley band to the Fermi level [see the green windows in Fig. 2(c)].

Furthermore, for P configuration in case for which $\Delta_\Omega \in [-(E_F + h + \Delta + \lambda_- - \lambda_+), -(E_F + \lambda_+ + h - \Delta + \lambda_-)] \cup [E_F + h - \Delta - \lambda_- - \lambda_+, E_F + \lambda_+ + h + \Delta - \lambda_-]$, i.e., $\Delta_\Omega \in [-2.925, -1.465] \cup [1.435, 3.375]$ and for AP configuration in case for which $\Delta_\Omega \in [-(E_F + h + \Delta - \lambda_- + \lambda_+), -(E_F - \lambda_+ + h - \Delta - \lambda_-)] \cup [E_F + h - \Delta + \lambda_- + \lambda_+, E_F - \lambda_+ + h + \Delta + \lambda_-]$, i.e., $\Delta_\Omega \in [-3.375, -1.435] \cup [1.465, 2.925]$ the Fermi level only intersects with one valley, leading to a fully valley polarization (valley filter) in the P and AP configurations as shown by purple windows in Figs. 2(b) and 2(c), respectively.

Figure 3 shows the contour plots of the transmission probabilities for the P and AP configurations as a function of incident angle ϕ and off-resonant light Δ_Ω. It is seen that the transmission is strongly spin-valley dependent and is very sensitive to the magnetization orientation of two ferromagnetic regions. The spin- and valley-polarized regions realized from the band structure in Figs. 2(b) and 2(c) can be further confirmed by the transmission curves in Figs. 3(a)–3(d) [Figs. 3(e)–3(h)] for the P (AP) magnetization orientations, which is essential for spin-valley filtering applications of the proposed asymmetric junction. In addition, from Fig. 3 we can see a symmetrical behavior in transmission with respect to the incident angle for all values of Δ_Ω.

It is demonstrated in Fig. 3 that reversing the polarity of light (the change sign of Δ_Ω) switches the transmission of opposite valleys at a given spin band. For instance, for P (AP) configuration for $T_{K\uparrow}$ ($T_{K\downarrow}$), we have the transmission in interval $\Delta_\Omega \in [-2.925, 1.435]$ ($\Delta_\Omega \in [-3.375, 1.465]$), which is obvious from Fig. 3(a) [Fig. 3(f)] and for $T_{K'\uparrow}$ ($T_{K'\downarrow}$), we have the transmission in interval $\Delta_\Omega \in [-1.465, 3.375]$ ($\Delta_\Omega \in [-1.435, 2.925]$), which is clear from Fig. 3(c) [Fig. 3(h)] and can be explained by the band structure in Figs. 2(b) and 2(c). Clearly, the asymmetry of transmission with respect to the sign of Δ_Ω in Fig. 3 reflects the asymmetry of band dispersion in Fig. 2.

After studying the transmission probability, as the conductance is a physical quantity and can be measured in the laboratory, we show the spin- and valley-resolved conductances as a function of Δ_Ω for two magnetization configurations in Figs. 4(a) and 4(b). For the P configuration,

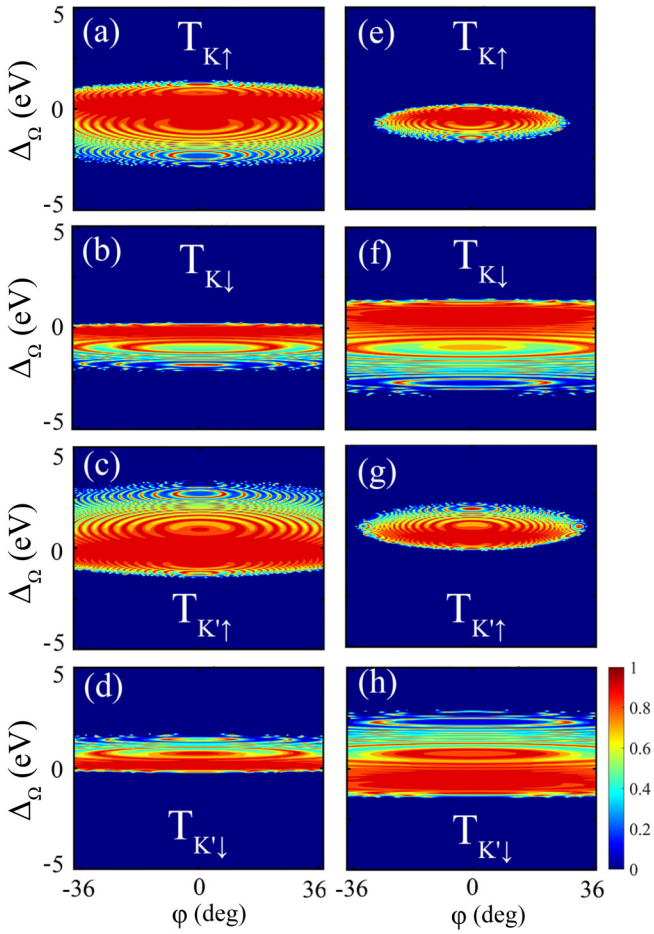

FIG. 3. Contour plots of the transmission probability through a WSe_2-based asymmetrical magnetic junction as functions of incident angle (ϕ) and off-resonant polarized light (Δ_Ω) for $L = 20$ nm and $h_1 = h_2 = 0.6$ eV. The left (right) column represents the results for P (AP) configuration.

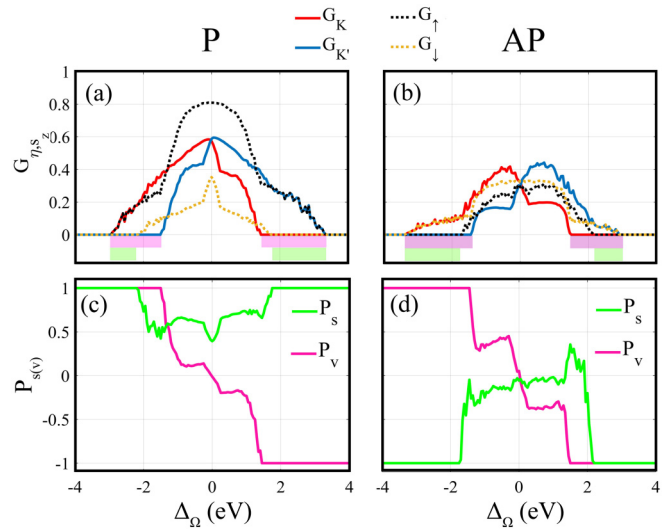

FIG. 4. (a), (b) Spin- and valley-resolved conductances vs Δ_Ω, (c), (d) valley (P_v) and spin (P_s) polarizations vs Δ_Ω for (a), (c) P and (b), (d) AP configurations. Here, $L = 20$ nm, $h_1 = h_2 = 0.6$ eV, and $E_F = 1.7$ eV.

the majority of the spin state (say, spin up) in both ferromagnetic regions is the same. So, the conductance associated with the spin-up electrons is bigger than spin down [see the dotted black and dotted orange curves in Fig. 4(a)]. For AP configuration, the majority-spin state in both ferromagnetic regions will be of the opposite type. So, majority-spin electrons (spin up) from left ferromagnetic can tunnel to minority-spin states (spin up) of the middle ferromagnetic, and minority-spin electrons (spin down) from the left ferromagnetic can tunnel to majority-spin states (spin down) of middle ferromagnetic. Consequently, $G_\downarrow$ for the AP configuration is bigger than $G_\uparrow$ [see the dotted black and dotted orange curves in Fig. 4(b)].

It is noteworthy that for the right-handed (left-handed) circularly polarized light in Figs. 4(a) and 4(b), the spin-valley polarization and valley polarization windows in the conductance curves for both P and AP configurations will appear in some ranges of Δ_Ω in agreement with the band structure in Figs. 2(b) and 2(c). Therefore, the spin-valley filtering behavior can also be found from the transmission and the measurable conductance.

Now, in order to further show the spin- and valley-polarized transport through the proposed asymmetric FFN WSe_2 junction, in Figs. 4(c) and 4(d), we have plotted the spin and valley polarizations as a function of Δ_Ω for both P and AP magnetization configurations. Since the conductance curves in some ranges of Δ_Ω is dominated only by one spin band from one valley, we have a fully spin-valley polarization in this proposed junction, as shown in Figs. 4(c) and 4(d). Clearly, by reversing the magnetization orientation from P to AP, the spin polarization (P_s) switches from 1 to -1, as seen in Figs. 4(c) and 4(d). This is due to the fact that reversing magnetization orientation is more effective on spin polarization because the spin plays the key role in reversing the magnetic orientation of the ferromagnetic region as can be seen from Eq. (1). Note also that in the absence of Δ_Ω we do not have valley polarization for both magnetization orientations. However, we have spin polarization for both configurations, which comes from the fact that the exchange field h breaks the spin degeneracy and gives rise to a nonzero spin polarization in the both P and AP configurations. From Figs. 4(c) and 4(d), it is seen that the valley polarization can be switched by the polarity of the off-resonance light. It means that we have $P_v = 1$ (-1) by using left-handed (right-handed) off-resonance light in the proposed FFN junction for both magnetization configurations, which is exactly confirmed by the band structure in Figs. 2(b) and 2(c).

Now, to show the effect of the gate voltage on the spin and valley polarizations, the contour plots of spin and valley polarizations as a function of U and Δ_Ω are presented in Fig. 5 for both P and AP configurations. Here, one can observe some outstanding phenomena for the polarizations:

(i) As can be seen in Figs. 5(a) and 5(b), the perfect valley polarization's direction is associated with the polarity of off-resonance light and by increasing the intensity of the off-resonance light for both polarities, the valley polarization can be realized in a larger range of gate voltage. Interestingly, in specific parameter regime, e.g., $U = E_F - |\Delta +$

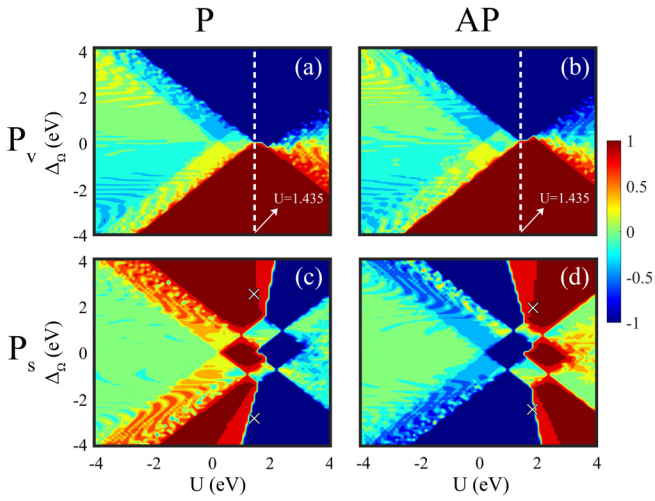

FIG. 5. Contour plot of (a), (c) spin polarization (P_s) and (b), (d) valley polarization (P_v) as a function of U and Δ_Ω. The top (bottom) panel is for P (AP) configurations. Note that the white symbols are at the same value of U. Other fixed parameters are the same as Fig. 4.

$\lambda_-| + h_2 - \lambda_+$, i.e., $U = 1.435$ eV (with $h_2 = h_1 = 0.6$ eV) we have the fully valley polarization for all values of Δ_Ω, in such a way that the valley polarization suddenly reversed by polarity of the light around $\Delta_\Omega \approx 0$ for both magnetization configurations.

(ii) The direction of the perfect spin polarization can be switched by U and magnetization orientation. As a result, we can see in Figs. 5(c) and 5(d) that at some specific values of U, the spin polarization can be switched from positive to negative values by reversing the polarity of light [see the white symbols in Figs. 5(c) and 5(d)]. This phenomenon mainly originates from the significant SOC in WSe_2, which allows the off-resonant light to interact with the spin conductances at specific U and leads to a new controlling method for the spin polarization. In fact, using the positive (negative) gate voltage can move the bands upward (downward), simultaneously. Thanks to the SOC of WSe_2, by applying an appropriate value of circularly polarized light ($\Delta_\Omega > 4\lambda_c = 30$ meV), the spin and valley degeneracies will be removed. So, using an appropriate value of U can single out a specific spin band to intersect with the Fermi level, leading to a perfect spin polarization which is switchable by the polarity of the light. This is the main reason for the fully spin-valley polarization which is optically and electrically tunable in Figs. 5(a)–5(d).

(iii) As can be seen in Figs. 5(c) and 5(d), in the absence of off-resonance light ($\Delta_\Omega = 0$) the fully spin polarization can be achieved for $E_F + |\Delta + \lambda_-| - \lambda_+ + h > U > E_F - |\Delta - \lambda_-| - h_2 + \lambda_+$, i.e., 2.925 eV $> U >$ 0.265 eV for both magnetization configurations, which arise from the exchange field. From Figs. 4 and 5 we conclude that due to the huge SOC of WSe_2, perfect spin polarization that is electrically and optically tunable and switchable is realized in the proposed asymmetric FFN junction. Tuning the sign and magnitude of the valley and spin polarization in monolayer WSe_2 by off-resonance light offers opportunities for control of the valley and spin degree of freedom for quantum information processing.

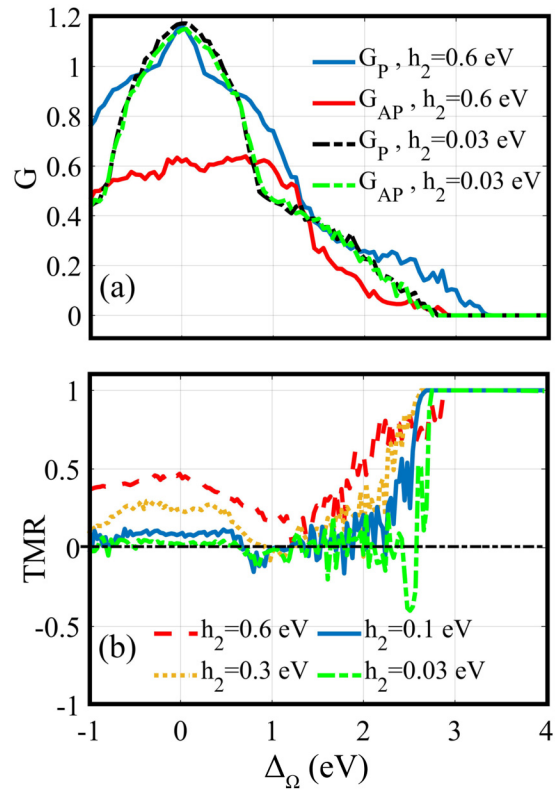

FIG. 6. (a) Total charge conductance as a function of Δ_Ω for both P and AP magnetization configurations and (b) TMR as a function of Δ_Ω for different h_2. Other parameters are the same as Fig. 4.

B. Tunneling magnetoresistance

Now, after calculating the spin and valley transports for both magnetization configurations, we discuss TMR effect in the proposed asymmetric FFN WSe_2 junction.

In Fig. 6(a) we plot the total conductance of the junction as a function of Δ_Ω for both P and AP configurations for $h_2 = 0.6$ and 0.03 eV. It is seen clearly that for all values of h_2 as Δ_Ω increases, the total charge conductances decrease and finally vanish, due to the migration of the Fermi level into the gap. Here, we can see that for the high exchange field ($h_2 = 0.6$ eV), the difference between G_P and G_{AP} increases. This is because, for the high exchange field, the imbalance between the majority- and minority-spin density of states in the middle ferromagnetic electrode increases. Consequently, for P (AP) configuration the majority- (minority-) spin electrons which tunnel through the low (high) magnetic barrier increases (decreases). Hence, the conductance difference for the P and AP configurations increases, leading to a positive TMR, as shown in Fig. 6(b). However, when the exchange field h_2 decreases, for $h_2 = 0.03$ eV, the difference between G_P and G_{AP} will be reduced, as seen in Fig. 6(a). The origin of this effect is that decreasing h_2 can reduce the imbalance between majority- and minority-spin density of states in the middle ferromagnetic electrode, resulting in decreasing G_P and G_{AP} difference. In this case, the fluctuations of the relative ratio of the spin-up (-down) density states' contributions to the P and AP conductances, which is due to the Δ_Ω, lead to steady phase shift for G_P and G_{AP} oscillation. So, both of

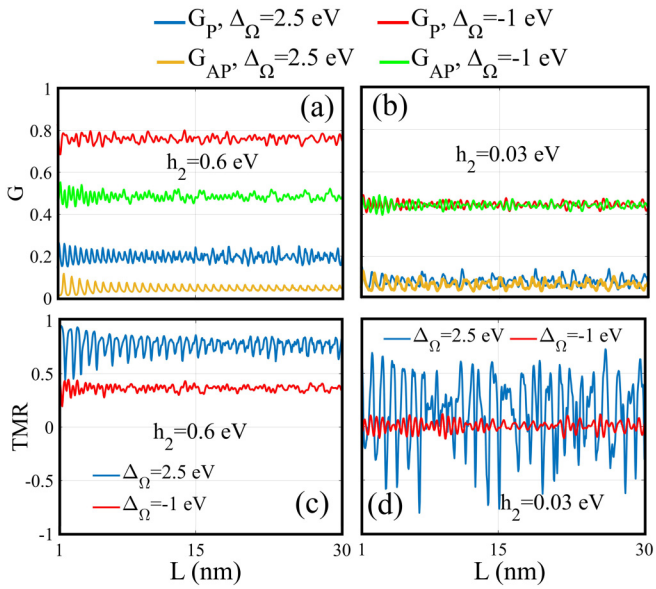

FIG. 7. (a) and (b) Total charge conductance as a function of L for both P and AP magnetization congurations and (c) and (d) TMR as a function of L for different Δ_Ω. In the left panel $h_2 = 0.6$ eV and in the right panel $h_2 = 0.03$ eV. Other fixed parameters are the same with Fig. 4.

them oscillate in antiphase with Δ_Ω, in such a way that the $G_{\rm P}$ and $G_{\rm AP}$ fluctuations will be sharpened at large Δ_Ω. Consequently, at some values of Δ_Ω, $G_{\rm AP}$ becomes bigger than $G_{\rm P}$, resulting in negative TMR, as seen in Fig. 6(b). We should emphasize that if we do similar calculations for FFN in MoS_2 (by setting $\lambda_+ = -\lambda_- = 0.0375$ eV, $v_f = 5.3 \times 10^5$ m/s, and $\Delta = 833$ meV for MoS_2) we see negative TMR also, that has not been reported in Ref. [23]. So, our results can be used for other TMDs such as MoS_2.

Furthermore, it must be emphasized that here we do not need a quantum well to see the negative TMR, as reported in ferromagnetic/insulator/normal/ferromagnetic (FINF) MoS_2 junction [25]. As shown in Fig. 6(b), when Δ_Ω becomes strong enough, $G_{\rm AP}$ goes to zero faster than $G_{\rm P}$ and this leads to TMR = 1 (saturation). In general condition, TMR can achieve the saturation value when $\Delta_\Omega \geqslant (E_F - \lambda_+ + h + \Delta + \lambda_-)$ because under this condition no band crosses the Fermi level for AP configuration. However, $K'_\downarrow$ band intersects with the Fermi level for P configuration, leading to $G_{\rm AP}$ vanishes faster than G_P. From Figs. 4 and 6 we conclude that by increasing the off-resonance light the TMR reaches 1, since at those values of Δ_Ω the junction is fully spin-valley polarized. This confirms that the TMR and spin-valley filtering effect of the proposed junction are optically tunable.

In Fig. 7 we explore the dependence of the total conductance and TMR on the middle ferromagnetic region's length (L) for two given Δ_Ω and exchange field h_2. One can see clearly that the conductance changes with L in an oscillatory way, which is due to the Klein tunneling of Dirac fermions [see Figs. 7(a) and 7(b)]. When the exchange field is strong enough the conductance for both values of Δ_Ω shows oscillatory behavior with L, with very small amplitude in a way that the $G_{\rm P}$ is always bigger than $G_{\rm AP}$ which leads to positive TMR, as shown in Figs. 7(a) and 7(c).

However, for weak exchange field, $G_{\rm P}$ and $G_{\rm AP}$ oscillate with L with different periods and phases [see Fig. 7(b)]. Consequently, the amplitude of $G_{\rm AP}$ oscillation is bigger than $G_{\rm P}$ at some values of L leads to a negative TMR, as shown in Fig. 7(d). Note that the amplitude of TMR oscillations becomes larger, when the off-resonance light increases (i.e., $\Delta_\Omega = 2.5$ eV). The oscillatory effect of the conductance curve is due to the Fabry-Perot resonance, which occurs by wavevector quantization. So, the lengths at which the resonances take place are given by

$$L_m = \frac{m\pi}{k'} = \frac{m\pi\hbar v_f}{\sqrt{(E - \eta s_z\lambda_+ + s_z h_2 - U)^2 - (\Delta + \eta\Delta_\Omega + \eta s_z\lambda_-)^2}}, \tag{7}$$

where m is an integer.

It is noteworthy that the negative TMR in this structure is induced by the combination of SOC, exchange field, and off-resonant polarized light, and the physical mechanism in this junction is totally different from that observed in FNF junctions based on graphene [17] and silicene [19], where the negative TMR comes from the change of the charge type in the right ferromagnetic electrode.

Finally, in the last figure, we are interested in exploring the effect of h_2 and Δ_Ω or L and Δ_Ω, simultaneously. In Fig. 8(a) we have shown the contour plot of TMR as a function of h_2 and Δ_Ω at $L = 20$ nm. It can be seen that this contour plot confirms the negative and positive values of TMR for the weak and strong exchange fields, respectively. Notice that for big enough Δ_Ω the TMR reaches 1 (saturation) for most values of h_2. Figures 8(b) and 8(c) present the contour plot of TMR versus L and Δ_Ω. As expected, the TMR for big exchange field ($h_2 = 0.6$ eV) is positive while for weak exchange field ($h_2 = 0.03$ eV) oscillates with L from negative to positive values. From Figs. 8(a)–8(c) it is obvious that by properly tuning the parameter regimes we can achieve positive TMR, negative TMR, and TMR = 1 in the proposed asymmetric FFN WSe_2 junction.

In our theoretical model, we can take the length of the middle FM region as a free parameter. However, in the real experiment, this length is practically fixed for each sample, therefore, varying the length of the layer in our theory implies creating several samples with different lengths for their middle FM region and performing TMR measurement for each of these samples. This is a challenging task in practice but feasible in principle with the available existing fabrication technology [49]. Our theory predicts that with the appropriately chosen length of the middle FM region, the remarkable sign change of the TMR may eventually be observed and applied for real spintronic and valleytronic devices.

As far as the experimental realization of such an asymmetric FFN junction in WSe_2 is concerned, it should be

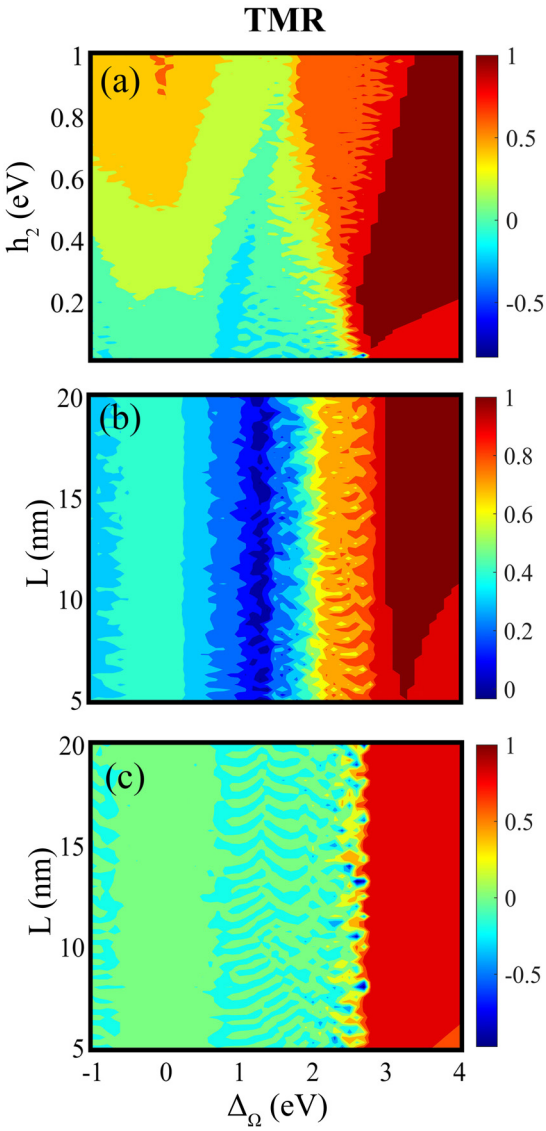

FIG. 8. (a) Contour plot of TMR vs h_2 and Δ_Ω for $L = 20$ nm. (b), (c) Contour plots of TMR vs L and Δ_Ω for (b) $h_2 = 0.6$ and (c) $h_2 = 0.03$ eV. Here, $U = 0$.

possible to fabricate such a structure with the currently available experimental techniques. The large (weak) ferromagnetic exchange field used in the left (middle) ferromagnetic region can be achieved by magnetic proximity effect using $BiFeO_3$ magnetic layer [50,51] (EuO) [52]. The optical properties of the proposed junction are of particular interest concerning valleytronics and possible device applications. In this regard, by optically pumping a MoS_2 with circularly polarized light and analyzing the subsequent photoluminescence for right and left helicities, one could measure the polarization of the light [30,31]. Also, to confirm a high degree of valley polarization of monolayer WSe_2, a circularly polarized excitation using a continuous wave laser at 660 nm (1.87 meV) has been used [53]. In our work, to see valley polarization in Figs. 4(a) and 4(b), we need a circularly polarized light (Δ_Ω) in the range of [1.43,3.37] for P and [1.46,2.92] for AP configurations which are in good agreement with those reported in the above experimental works.

A comment on the feasibility of observing the aforementioned phenomenon is worthwhile. In the absence of gate voltage, due to the intrinsic parameters of WSe_2 which are $\Delta = 850$ meV, $\lambda_c = 7.5$ and $\lambda_v = 112.5$ meV, considering the junction length of ∼10–30 nm, by setting $\Delta_\Omega \sim 1.88$ eV as reported in previous experimental studies [53] and irradiated by a helium-neon laser with ∼660 nm of wavelength, the perfect spin-valley polarization could be achievable by $h \sim 600$ meV. On the other hand, by reducing the exchange field to ∼30 meV, which is reported previously in graphene [52], in combination with $\Delta_\Omega \sim 1.5$–1.8 which can be generated by a long-wavelength laser of order 800 nm, the TMR oscillations switching may be observable as well practically.

IV. CONCLUSION

In summary, we have studied the spin and valley transports and TMR in asymmetry FFN WSe_2 junction in the presence of gate voltage and off-resonance light in the middle ferromagnetic region. Here, we propose fully spin- and valley-polarized currents for P and AP magnetization configurations by applying off-resonance light. The TMR can also be tuned to 1 in this junction by off resonance. Due to the strong SOC of WSe_2, the off-resonance light together with gate voltage switches the fully spin polarization, which has not been reported in the ferromagnetic-TMDs junctions available in literature. In addition, the fully valley and spin polarizations can be switched by the polarity of off-resonance light and the magnetization orientation of ferromagnetic regions, respectively. The relatively much stronger SOC in the conduction and valence bands of WSe_2 compared to other compounds of the dichalcogenides family accompanied by an off-resonance light leads to significant negative TMR at weak enough exchange fields. We have shown that in appropriate parameter regimes, the TMR of the proposed junction oscillates from negative to positive values and such a transition can be controlled by the off-resonance light. This work has revealed the potential of asymmetry WSe_2 junction for use as a spin-valley filter and magnetic tunneling junction.

ACKNOWLEDGMENTS

Y.H. thanks Shahid Chamran University of Ahvaz for financial support of this work under Grant No. SCU.SP99.100. I.M. thanks GREMAN, where this work was performed, for a work travel financial support useful to this research.

[1] K. Zollner, P. E. Faria Junior, and J. Fabian, Strain-tunable orbital, spin-orbit, and optical properties of monolayer transition-metal dichalcogenides, Phys. Rev. B **100**, 195126 (2019).

[2] Y. Liu, X. Duan, Y. Huang, and X. Duan, Two-dimensional transistors beyond graphene and TMDCs, Chem. Soc. Rev. **47**, 6388 (2018).

[3] H. Nan, R. Zhou, X. Gu, S. Xiao, and K. K. Ostrikov, Recent advances in plasma modification of 2 D transition metal dichalcogenides, Nanoscale **11**, 19202 (2019).

[4] K. F. Mak, C. Lee, J. Hone, J. Shan, and T. F. Heinz, Atomically Thin MoS_2: A New Direct-Gap Semiconductor, Phys. Rev. Lett. **105**, 136805 (2010).

[5] M. Tahir, P. M. Krstajić, and P. Vasilopoulos, Magnetic and electric control of spin-and valley-polarized transport across tunnel junctions on monolayer WSe_2, Phys. Rev. B **95**, 235402 (2017).

[6] X. Xu, W. Yao, D. Xiao, and T. F. Heinz, Spin and pseudospins in layered transition metal dichalcogenides, Nat. Phys. **10**, 343 (2014).

[7] D. Xiao, G.-B. Liu, W. Feng, X. Xu, and W. Yao, Coupled Spin and Valley Physics in Monolayers of MoS_2 and Other Group-VI Dichalcogenides, Phys. Rev. Lett. **108**, 196802 (2012).

[8] H.-Z. Lu, W. Yao, D. Xiao, and S.-Q. Shen, Intervalley Scattering and Localization Behaviors of Spin-Valley Coupled Dirac Fermions, Phys. Rev. Lett. **110**, 016806 (2013).

[9] R. Bertoni, C. W. Nicholson, L. Waldecker, H. Hübener, C. Monney, U. De Giovannini, M. Puppin, M. Hoesch, E. Springate, R. T. Chapman *et al.*, Generation and Evolution of Spin-, Valley-, and Layer-Polarized Excited Carriers in Inversion-Symmetric WSe_2, Phys. Rev. Lett. **117**, 277201 (2016).

[10] X.-J. Hao, R.-Y. Yuan, T. Ji, and Y. Guo, Switch effect for spin-valley electrons in monolayer WSe_2 structures subjected to optical field and Fermi velocity barrier, J. Appl. Phys. **128**, 154303 (2020).

[11] C. Zhao, T. Norden, P. Zhang, P. Zhao, Y. Cheng, F. Sun, J. P. Parry, P. Taheri, J. Wang, Y. Yang *et al.*, Enhanced valley splitting in monolayer WSe_2 due to magnetic exchange field, Nat. Nanotechnol. **12**, 757 (2017).

[12] K. L. Seyler, D. Zhong, B. Huang, X. Linpeng, N. P. Wilson, T. Taniguchi, K. Watanabe, W. Yao, D. Xiao, M. A. McGuire *et al.*, Valley manipulation by optically tuning the magnetic proximity effect in WSe_2/CrI_3 heterostructures, Nano Lett. **18**, 3823 (2018).

[13] X. Qiu, Q. Lv, and Z. Cao, Optical, electric and magnetic controlled ballistic conductance in monolayer WSe_2: the perfect valley and spin polarizations, J. Phys. D: Appl. Phys. **50**, 455106 (2017).

[14] W. H. Butler, Tunneling magnetoresistance from a symmetry filtering effect, Sci. Technol. Adv. Mater. **9**, 014106 (2008).

[15] H. Maehara, K. Nishimura, Y. Nagamine, K. Tsunekawa, T. Seki, H. Kubota, A. Fukushima, K. Yakushiji, K. Ando, and S. Yuasa, Tunnel magnetoresistance above 170% and resistance–area product of 1 $(\mu m)^2$ attained by in situ annealing of ultra-thin MgO tunnel barrier, Appl. Phys. Express **4**, 033002 (2011).

[16] J. S. Moodera, L. R. Kinder, T. M. Wong, and R. Meservey, Large Magnetoresistance at Room Temperature in Ferromagnetic Thin Film Tunnel Junctions, Phys. Rev. Lett. **74**, 3273 (1995).

[17] J. Zou, G. Jin, and Y.-q. Ma, Negative tunnel magnetoresistance and spin transport in ferromagnetic graphene junctions, J. Phys.: Condens. Matter **21**, 126001 (2009).

[18] C. Bai and X. Zhang, Large oscillating tunnel magnetoresistance in ferromagnetic graphene single tunnel junction, Phys. Lett. A **372**, 725 (2008).

[19] R. Saxena, A. Saha, and S. Rao, Conductance, valley and spin polarizations, and tunneling magnetoresistance in ferromagnetic-normal-ferromagnetic junctions of silicene, Phys. Rev. B **92**, 245412 (2015).

[20] D. Wang, Z. Huang, Y. Zhang, and G. Jin, Spin-valley filter and tunnel magnetoresistance in asymmetrical silicene magnetic tunnel junctions, Phys. Rev. B **93**, 195425 (2016).

[21] Y. Hajati and Z. Rashidian, Valley and spin resonant tunneling current in ferromagnetic/nonmagnetic/ferromagnetic silicene junction, AIP Advances **6**, 025307 (2016).

[22] Z. Rashidian, S. Rezaeipour, Y. Hajati, Z. Lorestaniweiss, and A. Ueda, Fully valley/spin polarized current and Fano factor through the graphene/ferromagnetic silicene/graphene junction, J. Magn. Magn. Mater. **424**, 207 (2017).

[23] X.-J. Qiu, Z.-Z. Cao, J. Hou, and C.-Y. Yang, Controlled giant magnetoresistance and spin–valley transport in an asymmetrical MoS_2 tunnel junction, Appl. Phys. Lett. **117**, 102401 (2020).

[24] M. Khezerlou and H. Goudarzi, Valley permitted Klein tunneling and magnetoresistance in ferromagnetic monolayer MoS_2, Superlattices Microstruct. **86**, 243 (2015).

[25] W.-T. Lu, H.-Y. Tian, H.-M. Liu, Y.-F. Li, and W. Li, Spin-and valley-dependent negative magnetoresistance in a ferromagnetic MoS_2 junction with a quantum well, Phys. Rev. B **98**, 075405 (2018).

[26] H. Rostami and R. Asgari, Valley Zeeman effect and spin-valley polarized conductance in monolayer MoS_2 in a perpendicular magnetic field, Phys. Rev. B **91**, 075433 (2015).

[27] L. Majidi, M. Zare, and R. Asgari, Valley-and spin-filter in monolayer MoS_2, Solid State Commun. **199**, 52 (2014).

[28] Z. Wang, C. Tang, R. Sachs, Y. Barlas, and J. Shi, Proximity-Induced Ferromagnetism in Graphene Revealed by the Anomalous Hall Effect, Phys. Rev. Lett. **114**, 016603 (2015).

[29] P. Lazić, K. D. Belashchenko, and I. Žutić, Effective gating and tunable magnetic proximity effects in two-dimensional heterostructures, Phys. Rev. B **93**, 241401(R) (2016).

[30] H. Zeng, J. Dai, W. Yao, D. Xiao, and X. Cui, Valley polarization in MoS_2 monolayers by optical pumping, Nat. Nanotechnol. **7**, 490 (2012).

[31] K. F. Mak, K. He, J. Shan, and T. F. Heinz, Control of valley polarization in monolayer MoS_2 by optical helicity, Nat. Nanotechnol. **7**, 494 (2012).

[32] T. Cao, G. Wang, W. Han, H. Ye, C. Zhu, J. Shi, Q. Niu, P. Tan, E. Wang, B. Liu *et al.*, Valley-selective circular dichroism of monolayer molybdenum disulphide, Nat. Commun. **3**, 887 (2012).

[33] Q. Yang, R. Yuan, and Y. Guo, Valley switch effect based on monolayer WSe_2 modulated by circularly polarized light and valley Zeeman field, J. Phys. D: Appl. Phys. **52**, 335301 (2019).

[34] M. Ezawa, Photoinduced Topological Phase Transition and a Single Dirac-Cone State in Silicene, Phys. Rev. Lett. **110**, 026603 (2013).

[35] T. Kitagawa, T. Oka, A. Brataas, L. Fu, and E. Demler, Transport properties of nonequilibrium systems under the application of light: Photoinduced quantum Hall insulators without Landau levels, Phys. Rev. B **84**, 235108 (2011).

[36] B. Dóra, J. Cayssol, F. Simon, and R. Moessner, Optically Engineering the Topological Properties of a Spin Hall Insulator, Phys. Rev. Lett. **108**, 056602 (2012).

[37] K. Saha, Photoinduced Chern insulating states in semi-Dirac materials, Phys. Rev. B **94**, 081103(R) (2016).

[38] M. Büttiker, Four-Terminal Phase-Coherent Conductance, Phys. Rev. Lett. **57**, 1761 (1986).

[39] T. Yokoyama, Controllable valley and spin transport in ferromagnetic silicene junctions, Phys. Rev. B **87**, 241409(R) (2013).

[40] T. Fujita, M. Jalil, and S. Tan, Valley filter in strain engineered graphene, Appl. Phys. Lett. **97**, 043508 (2010).

[41] V. H. Nguyen, A. Bournel, and P. Dollfus, Spin-polarized current and tunneling magnetoresistance in ferromagnetic gate bilayer graphene structures, J. Appl. Phys. **109**, 073717 (2011).

[42] J. S. Moodera and G. Mathon, Spin polarized tunneling in ferromagnetic junctions, J. Magn. Magn. Mater. **200**, 248 (1999).

[43] A. M. Jones, H. Yu, J. S. Ross, P. Klement, N. J. Ghimire, J. Yan, D. G. Mandrus, W. Yao, and X. Xu, Spin–layer locking effects in optical orientation of exciton spin in bilayer WSe_2, Nat. Phys. **10**, 130 (2014).

[44] A. Srivastava, M. Sidler, A. V. Allain, D. S. Lembke, A. Kis, and A. Imamoğlu, Valley Zeeman effect in elementary optical excitations of monolayer WSe_2, Nat. Phys. **11**, 141 (2015).

[45] A. F. Morpurgo and F. Guinea, Intervalley Scattering, Long-Range Disorder, and Effective Time-Reversal Symmetry Breaking in Graphene, Phys. Rev. Lett. **97**, 196804 (2006).

[46] E. McCann and V. I. Fal'ko, Symmetry of boundary conditions of the Dirac equation for electrons in carbon nanotubes, J. Phys: Condens. Matter **16**, 2371 (2004).

[47] K. Tran, A. Singh, J. Seifert, Y. Wang, K. Hao, J.-K. Huang, L.-J. Li, T. Taniguchi, K. Watanabe, and X. Li, Disorder-dependent valley properties in monolayer WSe_2, Phys. Rev. B **96**, 041302(R) (2017).

[48] B. Scharf, G. Xu, A. Matos-Abiague, and I. Žutić, Magnetic Proximity Effects in Transition-Metal Dichalcogenides: Converting Excitons, Phys. Rev. Lett. **119**, 127403 (2017).

[49] D. Gao, M. Si, J. Li, J. Zhang, Z. Zhang, Z. Yang, and D. Xue, Ferromagnetism in freestanding MoS_2 nanosheets, Nanoscale Res. Lett. **8**, 129 (2013).

[50] Y.-F. Wu, H.-D. Song, L. Zhang, X. Yang, Z. Ren, D. Liu, H.-C. Wu, J. Wu, J.-G. Li, Z. Jia *et al.*, Magnetic proximity effect in graphene coupled to a $BiFeO_3$ nanoplate, Phys. Rev. B **95**, 195426 (2017).

[51] Z. Qiao, W. Ren, H. Chen, L. Bellaiche, Z. Zhang, A. H. MacDonald, and Q. Niu, Quantum Anomalous Hall Effect in Graphene Proximity Coupled to an Antiferromagnetic Insulator, Phys. Rev. Lett. **112**, 116404 (2014).

[52] H.-X. Yang, A. Hallal, D. Terrade, X. Waintal, S. Roche, and M. Chshiev, Proximity Effects Induced in Graphene by Magnetic Insulators: First-Principles Calculations on Spin Filtering and Exchange-Splitting Gaps, Phys. Rev. Lett. **110**, 046603 (2013).

[53] K. Hao, G. Moody, F. Wu, C. K. Dass, L. Xu, C.-H. Chen, L. Sun, M.-Y. Li, L.-J. Li, A. H. MacDonald *et al.*, Direct measurement of exciton valley coherence in monolayer WSe_2, Nat. Phys. **12**, 677 (2016).